SUPPLEMENTARY INFORMATION

Crystal structure of the cytoplasmic N-terminal domain of subunit I, a homolog of subunit a, of V-ATPase

Sankaranarayanan Srinivasan[1]†, Nand K. Vyas[1]†, Matthew L. Baker[1,2] and Florante A. Quiocho[1]*

[1]*Verna and Marrs McLean Department of Biochemistry and Molecular Biology and* [2]*National Center for Macromolecular Imaging, Baylor College of Medicine, Houston, Texas 77030*

**Corresponding author*. Verna and Marrs McLean Department of Biochemistry and Molecular Biology Mail Stop BCM125, One Baylor Plaza Baylor College of Medicine Houston, TX 77030-3498. E-mail address: faq@bcm.edu

†Authors contributed equally to the work.

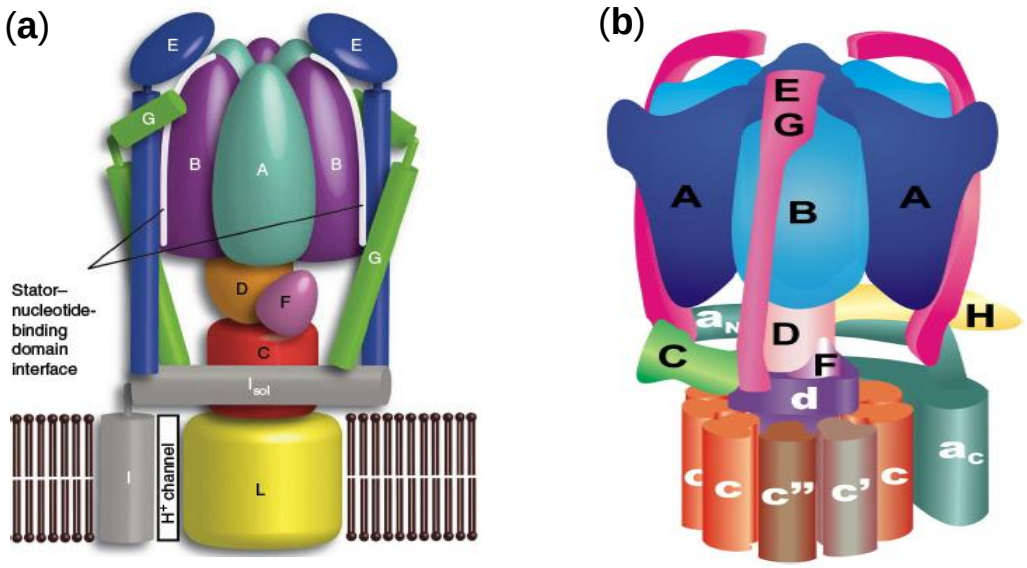

Fig. S1. Schematic of the architectures of (a) prokaryotic and (b) eukaryotic V-ATPases based on EM reconstructions. The figures are adapted with permission from the publishers. Equivalent subunits between cell types are listed in Table S1. (a) From the studies of *Thermus thermophilus* by Lee *et al*.[1] The cytoplasmic N-terminal domain of subunit I labeled "I_{sol}" is equivalent to I_{cyt} that has been adopted in our studies. This model was obtained by fitting crystal structures of all subunits and subcomplexes from bacteria (except subunit I). (b) From the investigation of yeast V-ATPase by Diepholz *et al*.[2] a_N is the N-terminal cytoplasmic domain of eukaryotic subunit "a" which is equivalent to a_{cyt} in the paper. With the exceptions of the known crystal structures of yeast subunits H and C, which are unique to eukaryotes, the equivalent crystal structures of bacterial subunits were used in the fitting. The crystal structure of subunit a, like its equivalent bacterial subunit I, is unknown.

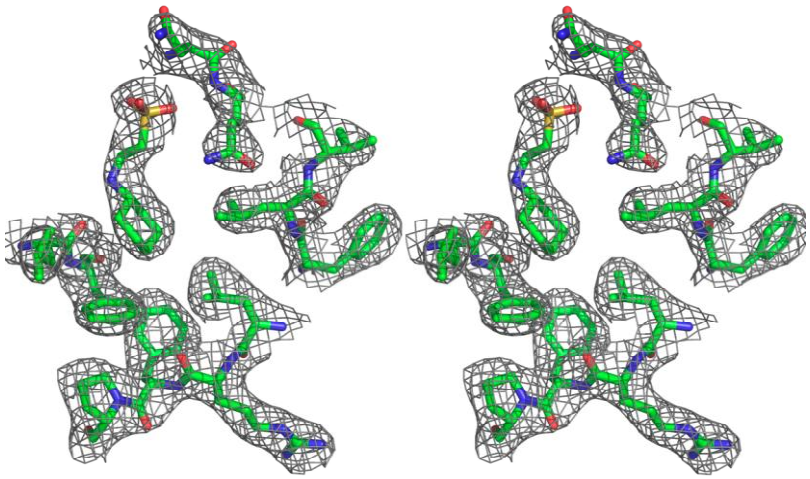

Fig. S2. Stereo diagram of representative electron density. Shown is a non-proteinaceous density into which a molecule of the crystallization buffer CHES (2-(Cyclohexylamino)ethanesulfonic acid) has been modeled and included in the refinement. Fully consistent with the nature of CHES, the cyclohexyl group is tucked in a hydrophobic pocket formed by residues Leu114 and Phe115 at C-terminal end of helix IV and Phe140, Leu141, Val142; Leu200, and Phe202 on loops of the distal lobe of the I_{cyt} structure. Moreover, polar residues Asn172 and Gln173 interact with the sulfonic group of CHES.

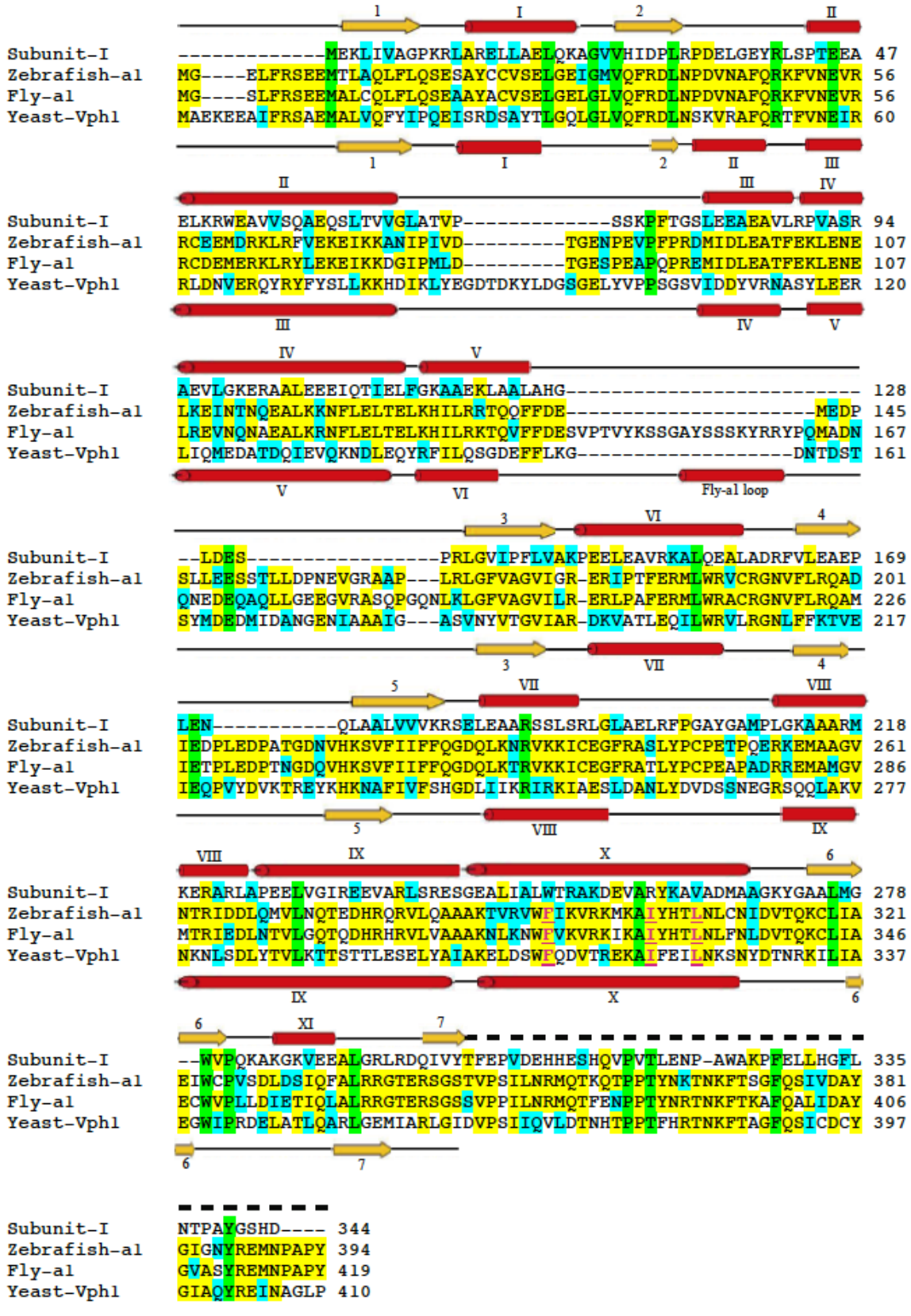
Subunit-I ----------MEKLIVAGPKRLARELLAELQKAGVVHIDPLRPDELGEYRLSPTEEA 47
Zebrafish-al MG----ELFRSEEMTLAQLFLQSESAYCCVSELGEIGMVQFRDLNPDVNAFQRKFVNEVR 56
Fly-al MG----SLFRSEEMALCQLFLQSEAAYACVSELGELGLVQFRDLNPDVNAFQRKFVNEVR 56
Yeast-Vph1 MAEKEEAIFRSAEMALVQFYIPQEISRDSAYTLGQLGLVQFRDLNSKVRAFQRTFVNEIR 60
Subunit-I ELKRWEAVVSQAEQSLTVVGLATVP----------SSKPFTGSLEEAEAVLRPVASR 94
Zebrafish-al RCEEMDRKLRFVEKEIKKANIPIVD---------TGENPEVPFPRDMIDLEATFEKLENE 107
Fly-al RCDEMERKLRYLEKEIKKDGIPMLD---------TGESPEAPQPREMIDLEATFEKLENE 107
Yeast-Vph1 RLDNVERQYRYFYSLLKKHDIKLYEGDTDKYLDGSGELYVPPSGSVIDDYVRNASYLEER 120
Subunit-I AEVLGKERAALEEEIQTIELFGKAAEKLAALAHG-------------------------- 128
Zebrafish-al LKEINTNQEALKKNFLELTELKHILRRTQQFFDE----------------------MEDP 145
Fly-al LREVNQNAEALKRNFLELTELKHILRKTQVFFDESVPTVYKSSGAYSSSKYRRYPQMADN 167
Yeast-Vph1 LIQMEDATDQIEVQKNDLEQYRFILQSGDEFFLKG-------------------DNTDST 161
Fly-al loop
Subunit-I --LDES----------PRLGVIPFLVAKPEELEAVRKALQEALADRFVLEAEP 169
Zebrafish-al SLLEESSTLLDPNEVGRAAP---LRLGFVAGVIGR-ERIPTFERMLWRVCRGNVFLRQAD 201
Fly-al QNEDEQAQLLGEEGVRASQPGQNLKLGFVAGVILR-ERLPAFERMLWRACRGNVFLRQAM 226
Yeast-Vph1 SYMDEDMIDANGENIAAAIG---ASVNYVTGVIAR-DKVATLEQILWRVLRGNLFFKTVE 217
Subunit-I LEN----------QLAALVVVKRSELEAARSSLSRLGLAELRFPGAYGAMPLGKAAARM 218
Zebrafish-al IEDPLEDPATGDNVHKSVFIIFFQGDQLKNRVKKICEGFRASLYPCPETPQERKEMAAGV 261
Fly-al IETPLEDPTNGDQVHKSVFIIFFQGDQLKTRVKKICEGFRATLYPCPEAPADRREMAMGV 286
Yeast-Vph1 IEQPVYDVKTREYKHKNAFIVFSHGDLIIKRIRKIAESLDANLYDVDSSNEGRSQQLAKV 277
Subunit-I KERARLAPEELVGIREEVARLSRESGEALIALWTRAKDEVARYKAVADMAAGKYGAALMG 278
Zebrafish-al NTRIDDLQMVLNQTEDHRQRVLQAAAKTVRVWFIKVRKMKAIYHTLNLCNIDVTQKCLIA 321
Fly-al MTRIEDLNTVLGQTQDHRHRVLVAAAKNLKNWFVKVRKIKAIYHTLNLFNLDVTQKCLIA 346
Yeast-Vph1 NKNLSDLYTVLKTTSTTLESELYAIAKELDSWFQDVTREKAIFEILNKSNYDTNRKILIA 337
Subunit-I --WVPQKAKGKVEEALGRLRDQIVYTFEPVDEHHESHQVPVTLENP-AWAKPFELLHGFL 335
Zebrafish-al EIWCPVSDLDSIQFALRRGTERSGSTVPSILNRMQTKQTPPTYNKTNKFTSGFQSIVDAY 381
Fly-al ECWVPLLDIETIQLALRRGTERSGSSVPPILNRMQTFENPPTYNRTNKFTKAFQALIDAY 406
Yeast-Vph1 EGWIPRDELATLQARLGEMIARLGIDVPSIIQVLDTNHTPPTFHRTNKFTAGFQSICDCY 397
Subunit-I NTPAYGSHD----- 344
Zebrafish-al GIGNYREMNPAPY 394
Fly-al GVASYREMNPAPY 419
Yeast-Vph1 GIAQYREINAGLP 410

Fig. S3. Amino acid sequence alignment of the cytosolic N-terminal domains from *M. ruber* subunit I (I_{cyt}) and three eukaryotic subunit a (a_{cyt}) homologs. The zebrafish and fly a1 orthologs are mainly neuronal in origin. Multiple sequence alignment was performed using ClustalW2. Invariant, identical and similar residues are highlighted in green, yellow and cyan, respectively. The secondary structures (α-helix, red cylinder and β-strand, yellow arrow) at the top are from the *M. ruber* I_{cyt} crystal structure (Fig. 1a), and those at the bottom are from I-TASSER,[3] the online threading program used to obtain the structure models of a_{cyt}s (see Methods and Table S3). Dashed lines at the C-terminal of I_{cyt} indicate a segment of residues which show no electron density (Fig. 1a and Methods) and assumed to be disordered in the a_{cyt} models. The secondary structures from I-TASSER agree very well with those obtained by the program PSI-PRED (data not shown). The I_{cyt} crystal structure and a_{cyt} models contain one extra non-equivalent α-helix (XI and II, respectively). The long loop in fly a1 composed of residues S142-P162 is absent in all other subunit "a" homologs. With the loop excluded, almost all eukaryotic homologs are ~50 residues longer than those of bacterial subunit I. The extra residues are mostly located in loops (see also Fig. 1c). Helices VIII and IX in the I_{cyt} crystal structure were predicted to form one long helix (αIX) in eukaryotic a_{cyt}s, which is shown in Fig. 1c. Although the sequence identities and similarities between I_{cyt} and a_{cyt} domains are somewhat low (Table S3), the alignment indicates very close secondary structure matching of the I_{cyt} crystal structure with those predicted for the a_{cyt}s. The conserved residues (F, I and L) underlined and colored red in a_{cyt}s αX helix are essential for binding Ca^{2+}-calmodulin.[4] The long segment consisting of coil 1 (helix III) and coil 2 (helices IV-V-VI) of eukaryotic a_{cyt} (identified by COILS[5]) has been demonstrated to bind t-SNARE protein syntaxin or SNAP25.[6] Recent evidence suggests that mutations of the residues in helix V in fly a1 abolish binding to syntaxin (unpublished data, Dr. P. Robin Hiesinger, University of Texas Southwestern Medical Center). Lack of sequence conservation between I_{cyt} and the eukaryotic a_{cyt}s in the segments that interacts with t-SNAREs and Ca^{2+}-calmodulin suggests that the SNARE and calmodulin binding properties of a_{cyt}s for membrane fusion would have evolved later in evolution.

Table S1. Subunit composition and mass of prokaryotic and eukaryotic V-ATPases[a]

Prokaryote (*T. thermophilus*)		Eukaryote (Yeast)	
V_1 sector			
Name	Mass (kDa)	Name	Mass (kDa)
A	64	A	70
B	54	B	58
-	-	C	44
D	25	D	29
E	21	E	26
F	12	F	13
G	13	G	13
-	-	H	54
V_0 sector			
Name	Mass (kDa)	Name	Mass (kDa)
I	72[b]	a	96
L	8	c	16
		c′	17
		c″	23
C	36	d	40
-	-	e	8

[a] The crystal structures of all subunits, except subunit I, of the bacterial V-ATPase subunits were used to fit the cryo-EM reconstruction density maps of prokaryotic V-ATPase resulting in the schematics depicted in Fig. S1A. Crystal structures of subunits C and H from *S. cerevisiae* were used for fitting into eukaryotic V-ATPase density.[7] The crystal structure presented here represents the first instance of a subunit "I" or "a" reported in the literature.

[b] The mass of *M. ruber* subunit I is 73 kDa with sequence identity and similarity of 53% and 69%, respectively, with that of the *T. thermophilus*.

Table S2. Kinks between α-helices in the linker of the I_{cyt} structure[a]

Location of kinks	Angle (deg.)	N_{term}	I_n	C_{term}	Local Sequence[b]
III-IV	29.8	V87	L	R89	84AEAVLR**P**VA
IV-V	55.6	L114	F	G116	111TIELF**G**KAA
VIII-IX	41.5	R223	L	A225	220ERARLA**P**EE
IX-X	57.8	E242	S	G244	239LSRES**G**EAL

[a] According to the classification by the studies of Langelaan *et al*.,[8] kinks in α-helices, especially those in membranes, could either be bends due to a change in helix axis direction with all residues staying helical or disruptions owing to a change in helix axis direction accompanied by a loss of helical character or the requisite main chain hydrogen bonds. The four kinks listed above from the two series of α-helices in the linker (see Text) are caused by disruptions.

[b] Disruptions in helices are often caused by the presence of prolines or glycines,[8] which are the case for the four major kinks in I_{cyt} (bold and underlined). The prolines and glycines are located at I_{n+2} and I_{n+1}, respectively, C-terminal to where the kinks occur at position I_n. Since the prolines and glycines are absent in the eukaryotic a_{cyt} region (Fig. S3), it is possible that the disruptions are transformed to bends in a_{cyt}s, resulting in continuous α-helices for the homologous helices III-IV-V and VIII-IX-X. For example, αVIII and αIX in the *M. ruber* I_{cyt} crystal structure (Fig. 1a) were predicted to form one long helix (αIX) in eukaryotic a_{cyt}s model (Fig. S3).

Table S3. Statistics of the amino acid sequence alignment of *M. ruber* I_{cyt} with its equivalent eukaryotic a_{cyt} domains and the predicted structure models obtained from threading

a_{cyt} domain	Sequence Comparison[a]		Quality of Predicted Model[b]	
	Identity (%)	Similarity (%)	C-Score	TM-Score
Zebrafish a1	18.0	34.1	-2.56	0.42±0.14
Fly a1	18.0	31.0	-3.38	0.34±0.11
Yeast Vph1	16.3	30.7	-3.19	0.36±0.12

[a] From pair wise amino acid sequence alignment of the cytosolic domains of *M. ruber* subunit I with neuronal subunit a1 of zebrafish and fly and yeast Vph1 using EMBOSS.[9] The sequence identities are 2.5 times higher than that between I_{cyt} and yeast subunit C (Fig. 1d). In contrast to the somewhat low values of the sequence identities and similarities, pair wise alignment between eukaryotic homologs, especially mammalian homologs, show much higher identities and similarities.[4] For example, the neuronal zebrafish and fly subunit a1 orthologs show 71% and 81% sequence identity and similarity, respectively (Fig. S3). Although the sequence identities of I_{cyt} and the a_{cyt}s are relatively low, the very high conservation of secondary structures (Fig. S3) facilitated the threading.

[b] From modeling using the online server I-TASSER (Methods and Fig. S3).[3] The quality of the generated models is based on two major criteria in I-TASSER, the C-score and the TM-score. These criteria indicate reasonable models with very similar overall topology and high degree of three-dimensional structure similarity, particularly the preservation of the secondary structures as seen in the *M. ruber* I_{cyt} crystal structure (Figs. 1a and c; Fig. S3.). The differences in the structures occur in loops partly because I_{cyt} has a shorter sequence (Fig. S3). Of the three a_{cyt} models, the zebrafish model (Fig. 1c) showed better statistics and hence used in our study.

Methods

Protein Expression and Purification

Genomic DNA from strain 21 of *Meiothermus ruber* was obtained from ATCC (35948D-5). The stretch of nucleotides of subunit "I", encoding amino acid residues M1 to D344 and representing the first half (or cytosolic domain "I_{cyt}") of the entire protein, were amplified using PCR and ligated in frame into pET-44 Ek/LIC vector (Novagen). The vector introduced 13 additional residues at the amino end after thrombin cleavage. After verification by DNA sequencing (Lone Star Labs), constructs were transformed into BL21(DE3) *E. coli* expression strain (Novagen). For protein expression, cells were grown at 37°C in either LB broth supplemented with 50 mg/ml ampicillin with shaking (220 rpm) or a minimal medium containing 50 mg/L seleno-methionine for production of seleno-methionine labeled protein. Cells were induced with 0.1 mM, isopropyl-β-D-thiogalactopyranoside (IPTG) at A_{600} of 0.6-0.8 and then grown at 16°C overnight with shaking. Cells were pelleted (3000g, 20 min) and then resuspended in 300 mM NaCl and 50 mM sodium phosphate, pH 7.0. The cell suspension was passed through a microfluidizer (Microfluidics) multiple times for cell lysis. The lysate was centrifuged at 36,000g for 30min at 4° C, and the supernatant was loaded onto pre-equilibrated Talon resin (Clonetech). Resin was washed with 10 column volumes of 10 mM imidazole, 300 mM NaCl and 50 mM sodium phosphate, pH 7.0. 1:50 ratio of thrombin (HTI): fusion protein was added to the resin and incubated with gentle shaking at room temperature for 2 hours. The protein was eluted in 300 mM NaCl and 50 mM sodium phosphate, pH 7.0 and then the buffer exchanged to 50 mM NaCl and 20 mM Tris-HCl, pH 8.0. Protein was bound to a pre-packed 5 ml HiTrap Q HP column (GE Healthcare) and eluted using a linear gradient of NaCl from 0.05 to 1 M. Fractions containing protein were pooled, concentrated by ultra-filtration and further purified using a Superdex-200 HR10/30 column (GE Healthcare) in 50 mM NaCl and 20 mM Tris-HCl, pH 8.0. Pooled fractions were concentrated by ultra-filtration. Protein concentrations were determined using A_{280} and a molar extinction coefficient (ε) of 30940 M^{-1} cm^{-1} obtained using ProtParam tool.[10]

Crystallization and structure determination

Crystals were grown by hanging drop vapor diffusion method, by mixing equal volumes of protein stock solution 10 mg/ml and the reservoir buffer of 0.2 M lithium sulfate, 0.8 M sodium-potassium tartrate and 0.1 M CHES, pH 9.5. Protein crystals grew in 2-3 days at 20°C Before data collection, protein crystals were cryoprotected by serial transfers into mother liquor containing 25% glycerol and then by rapid immersion in liquid N_2. Diffraction data of crystals of native and seleno-methionine variant I_{cyt} were collected on APS synchrotron beam line 19-ID and showed diffraction data to 2.6 Å (Table 1). Indexing, integration and scaling were carried out with HKL3000.[11] The PHENIX software suite was used for solving the structure.[12] Phasing was performed using the seleno-methionine substituted protein by the single-wavelength anomalous diffraction method using the phenix-autosol wizard.[13,14] Resulting phases were the starting point for automatic model building with phenix.autobuild.[15,16] Alternate model building and refinement were done with Coot[17] and phenix-refine,[18] respectively. Final refinement statistics and quality of the structure are summarized in Table 1. Figures were generated using PyMol (Schrodinger LLC).

Only residues 1 to 301 of I_{cyt} could be fit into the electron density. Mass spectrometric analysis of I_{cyt} crystals and protein in solution indicated a mass of 38847 Daltons, consistent with the cloned cytosolic region (residues 1 to 344), plus 13 additional residues at the N-terminus that originated from the plasmid. Taken together these indicate that the 13 additional residues and 43 residues at the C-terminus are disordered in the electron density.

a_{cyt} model

Coordinates of the *M. ruber* I_{cyt} was used as a starting template for obtaining structural models of the N-terminal cytoplasmic domains (a_{cyt}s) of zebrafish a1, fly a1 and yeast Vph1 using the online server I-TASSER (http://zhanglab.ccmb.med.umich.edu/I-TASSER/).[3] Since no electron density for I_{cyt} was observed beyond residue 301, the three a_{cyt} sequences aligned by CLUSTALW and ending at that corresponding residue (Fig. S3) were used as the input sequence. Sequence template alignments were generated using the program MUSTER, which is built into I-TASSER. The quality of the generated models was assessed in I-TASSER based on two major criteria, the C- and the TM-scores. C-score is calculated based on the significance of the threading alignments and the convergence of the I-TASSER simulations. C-scores typically range from -5 to 2, with higher scores reflecting a model of better quality. TM-score is a measure of structural similarity between the predicted model and the native or experimentally determined structure, with a value close to 0.5 indicating a model of correct topology. The results of the assessments for the three a_{cyt} models obtained in this experiment are shown in Table S3.

Fitting into EM reconstruction density maps

Fitting was performed using UCSF's Chimera[20] and Foldhunter.[21] Evaluation of the fitting was done with e2fhstat.py available in EMAN2.[22] Based on this evaluation, all the fits depicted in Fig. 2 were unique (99^{th} percentile for volume inclusion and real-space correlation) and yielded the following cross-correlation values. The fit (Fig. 2a) of the crystal structures of I_{cyt} and *T. thermophilus* subunits E&G heterodimer (PDB 3k5b) into the 16 Å cryo-EM reconstruction (EMDB ID 1888) of the *T. thermophilus* V-ATPase gave cross-correlation values of 0.9164 and 0.9279, respectively. The cross-correlations of the fit (Fig. 2b) of the zebrafish a1 a_{cyt} model structure obtained as described above (see also Fig. 1c and Table S3) and the x-ray structures of subunits H (PDB 1h08) and C (PDB 1u7l) into the density of the 25 Å negative stain EM reconstruction of the intact yeast V-ATPase (EMDB ID: 1640) were 0.8662, 0.8600 and 0.8725, respectively. Similar fitting into the 17 Å cryo-EM density of *Manduca sexta* (EMDB ID 1590) (Fig. 2c) yielded cross correlations of 0.8199 for the a_{cyt} model and 0.8828 and 0.8678 for subunits H and C, respectively.

References

1. Lee, L. K., Stewart, A. G., Donohoe, M., Bernal, R. A. & Stock, D. (2010). The structure of the peripheral stalk of Thermus thermophilus H+-ATPase/synthase. *Nat Struct Mol Biol* **17**, 373-8.
2. Diepholz, M., Venzke, D., Prinz, S., Batisse, C., Florchinger, B., Rossle, M., Svergun, D. I., Bottcher, B. & Fethiere, J. (2008). A different conformation for EGC

stator subcomplex in solution and in the assembled yeast V-ATPase: possible implications for regulatory disassembly. *Structure* **16**, 1789-98.
3. Zhang, Y. (2008). I-TASSER server for protein 3D structure prediction. *BMC Bioinformatics* **9**, 40.
4. Zhang, W., Wang, D., Volk, E., Bellen, H. J., Hiesinger, P. R. & Quiocho, F. A. (2008). V-ATPase V0 sector subunit a1 in neurons is a target of calmodulin. *J Biol Chem* **283**, 294-300.
5. Lupas, A., Van Dyke, M. & Stock, J. (1991). Predicting coiled coils from protein sequences. *Science* **252**, 1162-4.
6. Hiesinger, P. R., Fayyazuddin, A., Mehta, S. Q., Rosenmund, T., Schulze, K. L., Zhai, R. G., Verstreken, P., Cao, Y., Zhou, Y., Kunz, J. & Bellen, H. J. (2005). The v-ATPase V0 subunit a1 is required for a late step in synaptic vesicle exocytosis in Drosophila. *Cell* **121**, 607-20.
7. Muench, S. P., Trinick, J. & Harrison, M. A. (2011). Structural divergence of the rotary ATPases. *Q Rev Biophys*, 1-46.
8. Langelaan, D. N., Wieczorek, M., Blouin, C. & Rainey, J. K. (2010). Improved helix and kink characterization in membrane proteins allows evaluation of kink sequence predictors. *J Chem Inf Model* **50**, 2213-20.
9. Rice, P., Longden, I. & Bleasby, A. (2000). EMBOSS: the European Molecular Biology Open Software Suite. *Trends Genet* **16**, 276-277.
10. Gasteiger E., H. C., Gattiker A., Duvaud S., Wilkins M.R., Appel R.D., Bairoch A. (2005). *Protein Identification and Analysis Tools on the ExPASy Server*. John M. Walker (ed): The Proteomics Protocols Handbook, Humana Press.
11. Minor, W., Cymborowski, M., Otwinowski, Z. & Chruszcz, M. (2006). HKL-3000: the integration of data reduction and structure solution--from diffraction images to an initial model in minutes. *Acta Crystallogr D Biol Crystallogr* **62**, 859-866.
12. Adams, P. D., Afonine, P. V., Bunkoczi, G., Chen, V. B., Davis, I. W., Echols, N., Headd, J. J., Hung, L. W., Kapral, G. J., Grosse-Kunstleve, R. W., McCoy, A. J., Moriarty, N. W., Oeffner, R., Read, R. J., Richardson, D. C., Richardson, J. S., Terwilliger, T. C. & Zwart, P. H. (2010). PHENIX: a comprehensive Python-based system for macromolecular structure solution. *Acta Crystallogr D Biol Crystallogr* **66**, 213-221.
13. Terwilliger, T. C., Adams, P. D., Read, R. J., McCoy, A. J., Moriarty, N. W., Grosse-Kunstleve, R. W., Afonine, P. V., Zwart, P. H. & Hung, L. W. (2009). Decision-making in structure solution using Bayesian estimates of map quality: the PHENIX AutoSol wizard. *Acta Crystallogr D Biol Crystallogr* **65**, 582-601.
14. Zwart, P. H., Afonine, P. V., Grosse-Kunstleve, R. W., Hung, L. W., Ioerger, T. R., McCoy, A. J., McKee, E., Moriarty, N. W., Read, R. J., Sacchettini, J. C., Sauter, N. K., Storoni, L. C., Terwilliger, T. C. & Adams, P. D. (2008). Automated structure solution with the PHENIX suite. *Methods Mol Biol* **426**, 419-435.
15. Terwilliger, T. C. (2003). SOLVE and RESOLVE: automated structure solution and density modification. *Methods Enzymol* **374**, 22-37.
16. Terwilliger, T. C. (2002). Automated structure solution, density modification and model building. *Acta Crystallogr D Biol Crystallogr* **58**, 1937-1940.
17. Emsley, P., Lohkamp, B., Scott, W. G. & Cowtan, K. (2010). Features and development of Coot. *Acta Crystallogr D Biol Crystallogr* **66**, 486-501.

18. Afonine, P. V., Grosse-Kunstleve, R.W. & Adams, P.D. (2005). The Phenix refinement framework. *CCP4NewsI* **contribution8**.
19. Lau, W. C. & Rubinstein, J. L. (2010). Structure of intact Thermus thermophilus V-ATPase by cryo-EM reveals organization of the membrane-bound V(O) motor. *Proc Natl Acad Sci U S A* **107**, 1367-72.
20. Pettersen, E. F., Goddard, T. D., Huang, C. C., Couch, G. S., Greenblatt, D. M., Meng, E. C. & Ferrin, T. E. (2004). UCSF Chimera--a visualization system for exploratory research and analysis. *J Comput Chem* **25**, 1605-1612.
21. Jiang, W., Baker, M. L., Ludtke, S. J. & Chiu, W. (2001). Bridging the information gap: computational tools for intermediate resolution structure interpretation. *J Mol Biol* **308**, 1033-1044.
22. Tang, G., Peng, L., Baldwin, P. R., Mann, D. S., Jiang, W., Rees, I. & Ludtke, S. J. (2007). EMAN2: an extensible image processing suite for electron microscopy. *J Struct Biol* **157**, 38-46.